**Article:**
Khamtawi, R., Chureemart, J., Chantrell, R. W. et al. (2025) Enhanced giant magnetoresistance in Heusler alloy (Co2FeSi/Ag)N multilayers for read sensor applications. Journal of Physics D: Applied Physics. 085004. ISSN: 0022-3727

https://doi.org/10.1088/1361-6463/ad9bbe

Journal of Physics D:
Applied Physics



**PAPER** • **OPEN ACCESS**

# Enhanced giant magnetoresistance in Heusler alloy $(Co_2FeSi/Ag)_N$ multilayers for read sensor applications

To cite this article: R Khamtawi *et al* 2025 *J. Phys. D: Appl. Phys.* **58** 085004





OPEN ACCESS
IOP Publishing
Journal of Physics D: Applied Physics
J. Phys. D: Appl. Phys. **58** (2025) 085004 (9pp)
https://doi.org/10.1088/1361-6463/ad9bbe

# Enhanced giant magnetoresistance in Heusler alloy $(Co_2FeSi/Ag)_N$ multilayers for read sensor applications

**R Khamtawi[1], J Chureemart[1,2], R W Chantrell[1,2] and P Chureemart[1,2,*]**

[1] Department of Physics, Mahasarakham University, Mahasarakham 44150, Thailand
[2] School of Physics, Engineering and Technology, University of York, York YO10 5DD, United Kingdom

E-mail: phanwadee.c@msu.ac.th and pc536@york.ac.uk

Received 24 July 2024, revised 30 October 2024
Accepted for publication 8 December 2024
Published 27 December 2024

**Abstract**

We theoretically investigate the spin transport behavior of multilayer $[Co_2FeSi/Ag]_N$ structure for the application of next-generation read sensors in hard disk drive. To demonstrate the potential of the Heusler alloy-based current-perpendicular-to-plane giant magnetoresistance (CPP-GMR) device, we employ an atomistic model coupled with a spin accumulation model including the effect of a diffuse interface. The dynamics of magnetization is observed in the atomistic model and the calculation of magnetoresistance (MR) and MR ratio of the magnetic structure can be achieved by the spin accumulation model enabling us to investigate the spin transport behavior within the structure. The MR value can be directly calculated from the gradient of spin accumulation and spin current. The effect of injected current density is first investigated. It is found that increasing the current density results in a high MR ratio. Subsequently, to achieve a high performance reader, the number of coupled layers ($N$) is varied up to 16 to study its effect on the MR ratio. The calculated results indicate that increasing the number of layers $N$ gives rise to the enhancement of the resistance change and MR ratio. At the critical point $N = 5$, further increasing $N$ does not affect the MR ratio, which remains relatively unchanged. Interestingly, the MR ratio is doubled for $N > 5$ compared to $N = 1$. Our results demonstrate the possibility of enhancing the performance of multilayer CPP-GMR devices.

Keywords: Heusler alloy multilayer system, atomistic model, spin accumulation model, spintronic devices

## 1. Introduction

Presently, there is a demand to increase the data capacity of hard disk drives (HDDs) beyond 2.5 Tbit/in$^2$, emphasizing the necessity for enhanced storage solutions [1–5]. This demand is driven by the anticipation of the data growth rate surpassing 175 ZB (zettabytes) by 2025 [6, 7]. To further develop high-performance HDDs to meet this requirement, high-efficiency writing and reading technologies are needed to deal with small data bits. The read element leverages the benefits of the spin valve (SV) structure, which is a sandwich of two ferromagnetic materials (FMs) separated by a nonmagnet. The first FM functions as a pinned layer where the magnetization is fixed via the exchange bias phenomenon, while the second FM serves as a free layer (FL) where the magnetization is freely rotated. In the readout process, the SV produces a readback signal

* Author to whom any correspondence should be addressed.

corresponding to the change in magnetoresistance ($\Delta$MR) between the parallel and anti-parallel (AP) configurations of magnetization. Efficiently detecting the correct readback signal has become a challenging task in designing an appropriate reader for small data bit sizes [6, 8–12].

For HDDs with a capacity beyond 2 $Tb/in^2$, the tunneling MR (TMR) read-head does not meet the criteria due to the large resistance-area (RA) product, leading to high power dissipation. Alternatively, a current-perpendicular-to-plane giant MR (CPP-GMR) reader, using promising materials such as Heusler alloys and 2D materials is proposed as a solution, offering low RA and a high MR ratio [13, 14]. The conventional trilayer SV with Heusler alloy demonstrates strong performance in terms of thermal stability and high MR ratio at room temperature. However, the shrinking size of the reader affects the sensitivity and enhances the RA product to over 100 $f\Omega{\cdot}m^2$, resulting in the reduction of the MR ratio, increased power consumption and the potential for noisy device operation. Since the MR ratio is related to the spin-dependent scattering in the regions of the interface and bulk [15–23], the multilayer system has been proposed to improve MR ratio to address these limitations associated with the large number of interfaces.

The CPP-GMR multilayer stack was initially studied in the $[Fe/Cr]_N$ system where $N$ represents the number of coupled layers. The findings indicate that the shunting of bilayers results in a greater MR ratio and lower RA product compared to the conventional system [24–28]. In addition, the CPP-GMR multilayer structures employing conventional FM, such as the system of $[Co/Cu]_N$ [29–35], $[Fe/Cu]_N$ [31], $[Ni/Cu]_N$ [35–37] and $[NiFe/Cu]_N$ [38], have been extensively studied. However, the conventional multilayer system gives GMR ratio 25% at room temperature that is unable to achieve the desired high MR ratios for reader applications and susceptible to thermal instability because of high RA product [39–42]. To overcome these challenges, it is important not only to design the appropriate reader structure but also to choose materials with high spin transport properties, which has emerged as a key factor. Heusler alloys have become promising candidate materials with high magnetic and transport properties. In particular, Co-based Heusler alloys have been of considerable interest in read sensor applications, as evidently demonstrated their capability to enhance the performance of read sensors in previous studies [43–50]. $Co_2$-based Heusler compounds, such as $Co_2FeSi$ (CFS), exhibit remarkable magnetic properties, including high Curie temperatures of approximately 1100 K and large magnetic moments of 6 $\mu_B/f.u.$ [51], which significantly enhance their applicability in magnetic recording storage and spintronic devices. CFS is a distinctive full Heusler alloy exhibiting the rare properties of half-metallic ferromagnetism. This property is crucial for spintronic applications, as it provides nearly 100% spin polarizations at the Fermi level [51–54]. Such high spin polarization greatly enhances spin transport behavior, making CFS highly desirable for advanced spintronics.

To enhance reader performance and support future recording technology, utilizing Heusler alloys in multilayer SVs could be a promising alternative pathway. While there have been several experimental and theoretical investigations [43, 44, 49, 55], intensive studies on multilayer systems with Heusler alloys, particularly in computational modeling, have received little attention. Therefore, in this work, a combination of atomistic model and spin accumulation model are specifically used to investigate the spin transport behavior in the multilayer system of Co-based Heusler alloy CPP-GMR, specifically $[CFS/Ag]_N$. CFS possesses high magnetization, a high spin polarization parameter of conductivity ($\beta$), and a high Curie temperature ($T_c$). Ag, which is a good conductor and known to support good spin transport, plays an important role as a spacer layer in magnetic multilayer systems. Its high conductivity and long spin diffusion length ($\lambda_{sdl}$) allow the spin-polarized current to flow easily through the structure. The Ag layer helps to preserve the spin-polarized current flowing between ferromagnetic layers and to protect the interaction with adjacent ferromagnetic layers. Additionally, Ag helps to reduce the RA product, improve the MR ratio and enhance device performance. The CFS/Ag system is considered in this work because the band matching between CFS and Ag plays a crucial role in minimizing spin scattering at the interface, which allows efficient spin transport from CFS to Ag, as demonstrated in previous studies [43, 56, 57]. The structure of $[CFS/Ag]_N$, with the repetitions of $N = 16$, is studied to optimize the design of a suitable read sensor with small size and high performance.

## 2. Methodology

To develop and improve the performance of a read sensor, it is essential to understand the underlying spin transport behavior within the magnetic structure that governs the operation of the device. The methodology employed in this work relies on two models: the spin accumulation model and the atomistic model [58–65]. The spin accumulation model is applied to describe the spin transport behavior within a magnetic structure involving physical quantities such as spin accumulation and spin current. Meanwhile, an atomistic model is used to observe the dynamics of magnetization under the influence of the spin transfer torque (STT).

The CPP-GMR sensor functions through the introduction of a charge current perpendicular to the plane of the structure. The spin of the conduction electrons flowing into the magnetic structure interacts with the local spin moment of the ferromagnet, thereby exerting spin transfer torque on the local spin moment. The effect of STT can be described via the s-d exchange interaction between the spin accumulation ($\vec{m}$) and the local spin moment ($\mathbf{S}$). The energy of this interaction is given by, $\mathcal{H}_{STT} = -J_{sd}\vec{m}\cdot\mathbf{S}$. Subsequently, the STT field acting on the local spin moment can be derived from the negative first derivative of the s-d exchange energy as follows,

$$\mathbf{B}_{STT} = -J_{sd}\vec{m} \tag{1}$$

where $J_{sd}$ denotes the exchange integral of the s-d exchange interaction. The self-consistent solution of spin accumulation

for any arbitrary direction of local spin moment can be considered in the rotated coordinate system ($\hat{\mathbf{b}}_1$, $\hat{\mathbf{b}}_2$ and $\hat{\mathbf{b}}_3$) where $\hat{\mathbf{b}}_1$ is parallel with the direction of the local spin moment. The direction of $\hat{\mathbf{b}}_2$ and $\hat{\mathbf{b}}_3$ are perpendicular to the local spin moment. Therefore, the solution of spin accumulation is divided into two main parts: longitudinal ($\mathbf{m}_{\parallel}$) and transverse components ($\mathbf{m}_{\perp,2}$ and $\mathbf{m}_{\perp,3}$) as shown in the following form [56, 66–69],

$$\begin{aligned}\mathbf{m}_{\parallel}(x) &= \left[m_{\parallel}(\infty) + \left[m_{\parallel}(0) - m_{\parallel}(\infty)\right] \mathrm{e}^{-x/\lambda_{\mathrm{sdl}}}\right] \hat{\mathbf{b}}_1 \\ \mathbf{m}_{\perp,2}(x) &= 2\mathrm{e}^{-k_1 x}\left[u\cos(k_2 x) - v\sin(k_2 x)\right] \hat{\mathbf{b}}_2 \\ \mathbf{m}_{\perp,3}(x) &= 2\mathrm{e}^{-k_1 x}\left[u\sin(k_2 x) + v\cos(k_2 x)\right] \hat{\mathbf{b}}_3, \end{aligned} \tag{2}$$

with the coefficients $(k_1 \pm ik_2) = \sqrt{\lambda_{\mathrm{sf}}^{-2} \pm i\lambda_J^{-2}}$. Here, $m_{\parallel}(\infty)$ represents the spin accumulation at equilibrium, where the spin-flip length is defined as $\lambda_{\mathrm{sf}} = \sqrt{2D_0\tau_{\mathrm{sf}}}$, and $\lambda_{\mathrm{J}}$ denotes the spin-precession length. The variables $u$, $v$, and $m_{\parallel}(0)$ are derived by applying the spin current boundary condition across interfaces. The spatial variation of the spin current can be calculated from the below equation,

$$\mathbf{j}_m(x) = \beta j_e \mathbf{S} - 2D_0\left[\frac{\partial \vec{\mathrm{m}}}{\partial x} - \beta\beta' \mathbf{S}\left(\mathbf{S}\cdot\frac{\partial \vec{\mathrm{m}}}{\partial x}\right)\right], \tag{3}$$

where $\mathbf{S}$ is the unit vector of the local spin moment, $\beta$ and $\beta'$ are the spin polarization parameter of the material, $j_e$ is the charge current density and $D_0$ are the diffusion constant.

The influence of STT on the dynamics of local spin moments can be directly evaluated from the calculated spin accumulation, as detailed earlier. To observe the dynamics of local spin moments in the presence of STT, the Landau–Lifshitz-Gilbert (LLG) equation is utilized as outlined below [70]:

$$\frac{\partial \mathbf{S}}{\partial t} = -\frac{\gamma}{(1+\alpha^2)}(\mathbf{S}\times\mathbf{B}_{\mathrm{eff}}) - \frac{\gamma\alpha}{(1+\alpha^2)}\left[\mathbf{S}\times(\mathbf{S}\times\mathbf{B}_{\mathrm{eff}})\right] \tag{4}$$

where $\mathbf{S}$ is the normalized atomic spin vector, $\gamma$ is the absolute value of the gyromagnetic ratio and $\alpha$ is the intrinsic damping constant. The effective field acting on each atomic spin, denoted as $\mathbf{B}_{\mathrm{eff}}$, consisting of the contribution from the exchange field, the anisotropy field, the externally applied field, the STT field, the demagnetizing field and the thermal field can be written as,

$$\begin{aligned}\mathbf{B}_{\mathrm{eff}} &= \mathbf{B}_{\mathrm{exch}} + \mathbf{B}_{\mathrm{ani}} + \mathbf{B}_{\mathrm{app}} + \mathbf{B}_{\mathrm{STT}} + \mathbf{B}_{\mathrm{demag}} + \mathbf{B}_{\mathrm{th}} \\ &= \sum_{i<j} J_{ij}\mathbf{S}_j + 2k_{\mathrm{u}}\sum_i (\mathbf{S}_i\cdot\mathbf{e})\,\mathbf{e} + \mathbf{B}_{\mathrm{app}} + J_{\mathrm{sd}}\vec{\mathrm{m}} \\ &\quad + \mathbf{B}_{\mathrm{demag}} + \mathbf{B}_{\mathrm{th}}\end{aligned} \tag{5}$$

where $\mathbf{S}_{i,j}$ is the unit vector of spin on site $(i,j)$, $J_{ij}$ is the nearest neighbor exchange integral between the spin sites $i$ and $j$, $k_{\mathrm{u}}$ is the uniaxial anisotropy constant and $\mathbf{e}$ is the unit vector of easy axis. The final two terms on the right side of equation (5) can be individually determined, as detailed below.

To reduce the computational time, the model considers the demagnetizing field and thermal fluctuations separately by using the macro-cell approach. The system is divided into many macro-cells, where the local spin moment within each cell is assumed to be uniform and the demagnetizing field of each local spin moment in that cell (denoted by $k$) is homogeneous, as given by,

$$\mathbf{B}_{\mathbf{demag},k} = \frac{\mu_0}{4\pi}\sum_{l\neq k}\left[\frac{3(\boldsymbol{\mu}_l\cdot\hat{\mathbf{r}}_{kl})\hat{\mathbf{r}}_{kl} - \boldsymbol{\mu}_l}{|r_{kl}|^3}\right], \tag{6}$$

and the magnetic moment vector in the macro-cell $l$, containing $n_{\mathrm{atom}}$ spins, is expressed as:

$$\boldsymbol{\mu}_l = \sum_{i=1}^{n_{\mathrm{atom}}} \mu_{\mathrm{s}}^i \mathbf{S}_i\,. \tag{7}$$

where $\mu_0$ is the permeability of free space, $r_{kl}$ and $\hat{\mathbf{r}}_{kl}$ are the distance and unit vector between macro-cell $k$ and $l$.

Furthermore, the model includes the thermal field acting on spin $i$ as a random field drawn from a Gaussian distribution as follows,

$$\mathbf{B}_{\mathrm{th,i}} = \Gamma(t)\sqrt{\frac{2\alpha k_{\mathrm{B}}T}{\gamma\mu_s\Delta t}}, \tag{8}$$

where $\Gamma(t)$ is obtained from a Gaussian distribution, $k_{\mathrm{B}}$ is the Boltzmann constant, $T$ is temperature, $\Delta t$ is the integration timestep and $\alpha$ denotes the damping constant.

The dynamics of magnetization in the presence of STT can be efficiently represented by integrating the total field into the LLG equation, which can be numerically solved using the Huen scheme. This approach offers a comprehensive insight into the dynamic behavior of the magnetization within the magnetic structure. Furthermore, the spin transport efficiency can be explained through the $(\mathrm{RA}_i)$ product at each position within the system. This value can be calculated directly from the gradient of spin accumulation $(\Delta m)$ and spin current $(j_m)$. To obtain the overall spin transport efficiency, the total RA product of the system is determined by summing the spatial $\mathrm{RA}_i$ values across all microcells given by,

$$\mathrm{RA}_{\mathrm{total}} = \sum_{i=1}^{n}\mathrm{RA}_i = \frac{V_{\mathrm{cell}}k_{\mathrm{B}}T}{e^2}\sum_{i=1}^{n}\frac{|\Delta m|}{|jm|} \tag{9}$$

where $n$ is the number of microcells, $V_{\mathrm{cell}}$ is the microcell volume and $e$ is the electron charge. The MR ratio is then evaluated from the RA of the parallel and AP states.

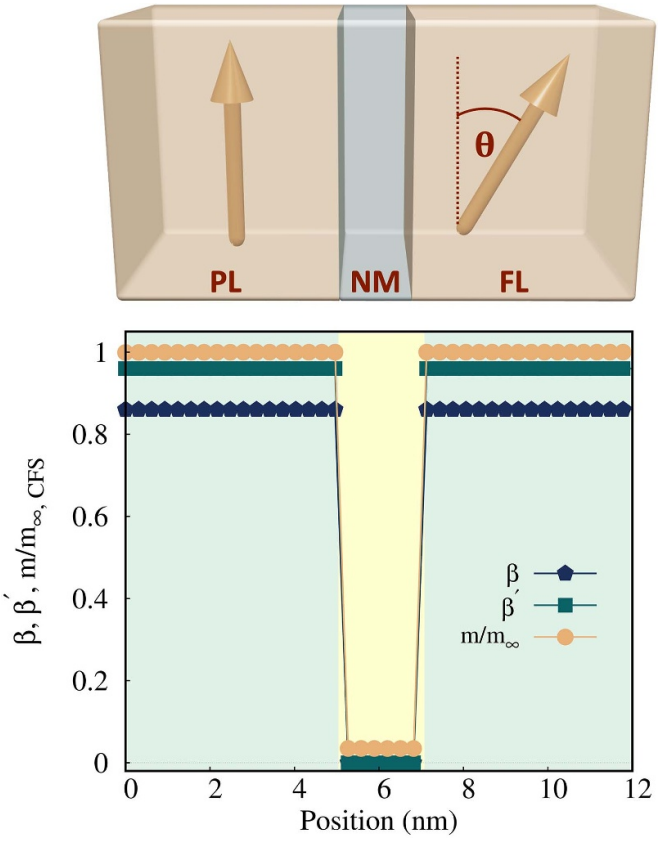


**Figure 1.** Schematic of the trilayer system CFS/Ag/CFS.

## 3. Results and discussions

In this section, we investigate giant MR (GMR) in SV structures by examining spin transport behavior in magnetic materials. Using a spin accumulation model induced by an injected charge current, the study first focuses on structures with two ferromagnetic layers separated by a nonmagnet. Specifically, the Heusler alloy system of $Co_2FeSi$ (CFS)/Ag/CFS is utilized. The effect of current density ranging from 1 to 5 mA $cm^{-2}$ on MR is considered. The study then examines spin transport in multilayer structures of $(CFS/Ag/CFS)_N$ and evaluates the impact of the number of layers $N$ on the MR as detailed below.

### 3.1. Spin transport behavior in the SV structure

We investigate the spin transport behavior within the SV structure of CFS/Ag/CFS, which can be carried out by employing the atomistic model along with the spin accumulation model. Initially, we focus on examining the spin transport behavior within the CFS(5 nm)/Ag(2 nm)/CFS(5 nm) trilayer system including a diffuse interface of 1 nm width as shown in figure 1. The magnetic and transport parameters of the material used in this work are detailed in table 1. For a realistic system, the interfacial region resulting from the intermixing between ions of two different materials is taken into account

**Table 1.** Spin transport parameters of CFS and Ag taken from references [71–73].

| Parameters | CFS | Ag |
|---|---|---|
| Spin polarization parameter for the conductivity ($\beta$) | 0.96 | 0 |
| Spin polarization parameter for the diffusion constant ($\beta'$) | 0.86 | 0 |
| Spin diffusion length ($\lambda_{sdl}$) | 1.7 nm | 160 |
| The s-d exchange interaction constant ($J_{sd}$) | 0.1 eV | 0 |
| The equilibrium value of spin accumulation ($m_\infty$) | 15.71 MC $m^{-3}$ | 0 |

in the model by using Fick's law [66–68, 74]. The spatial variation of the diffusive transport parameter, $P(x)$, can be considered by employing a linear combination of the bulk parameters weighted by the local concentrations in the following equation,

$$P(x) = P_A C_A(x) + P_B[1 - C_A(x)], \tag{10}$$

where $P_{A,B}$ is the diffusive transport parameter of ion $A$ or $B$. The position dependence of ion concentration $A$, originating from the intermixing of two different ion species at the interface, can be calculated using a given equation,

$$C_A(x) = \frac{N_A(x)}{[N_A(x) + N_B(x)]} \tag{11}$$

where $N_{A,B}(x)$ is the number of local ions $A$ and $B$ at any position $x$, obtained from the solution of Fick's law. This enables us to consider the spin transport parameters at any given position based on the concentration of magnetic ions. The spin transport parameters, which are $\beta$, $\beta'$, $\lambda_{sdl}$ and $J_{sd}$, remain unchanged at the position far away from the interface and they become gradually changed across the interface to reach the spin transport value of Ag as demonstrated in figure 1. This is due to the different spin transport values across the interface of CFS/Ag. The spin transport behavior can be described by physical quantities: spin accumulation and spin current at any given position. Subsequently, the obtained results for the trilayer system are compared with those of the multilayer system, providing a comprehensive understanding of the enhancement in read sensor performance.

Firstly, the effect of the relative angle, which is the angle between the magnetizations of two ferromagnets, is studied by varying the angle in the range $0 < \theta < 2\pi$. A charge current with the density of $j_e = 5\,\mathrm{mA\,cm^{-2}}$ is applied to a trilayer system consisting of CFS(5 nm)/Ag(2 nm)/CFS(5 nm) in order to investigate spin transport behavior, particularly focusing on spin accumulation and spin current. As demonstrated in figure 2, spin accumulation remains constant in the region far from the interface corresponding to the value of the spin transport parameters, and gradually changes across the first interface of CFS/Ag. In the second interface region, the spin

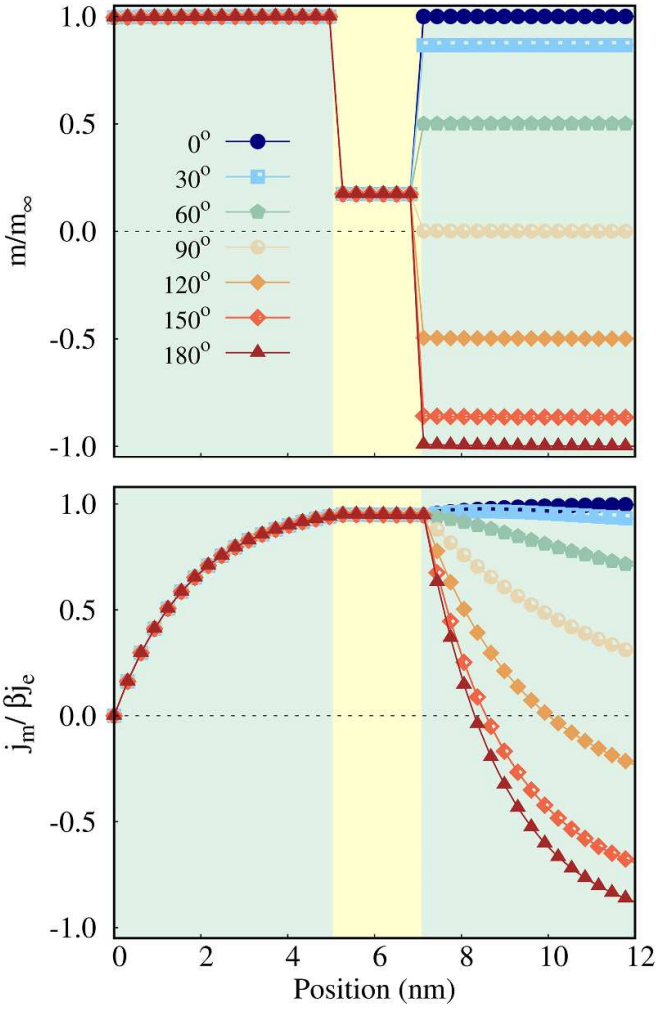


**Figure 2.** The spatial variation of spin accumulation and spin current in the trilayer system with different relative angle between two ferromagnets.

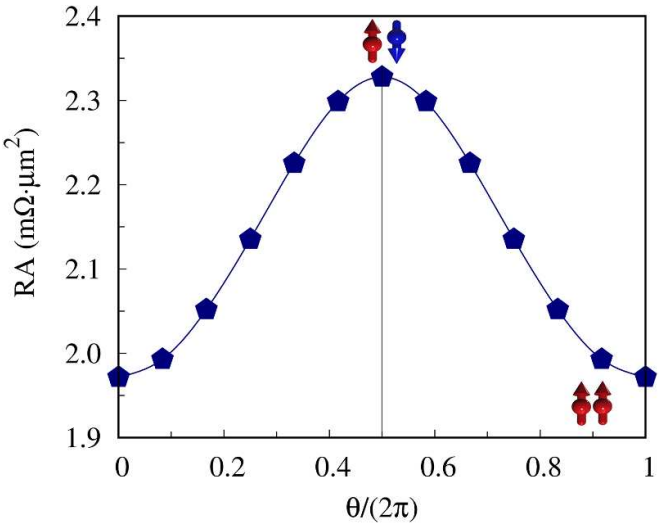


**Figure 3.** The angular dependence of resistance-area product (RA) in the system of CFS(5 nm)/Ag(2 nm)/CFS(5 nm) with injected current density of 5 mA cm$^{-2}$ .

accumulation tends to develop in the direction of magnetization. Similarly, the spin current is polarized and increased in the first CFS while remaining relatively constant within the Ag layer. Then, the spin polarized current tends to align in the direction of magnetization in the second CFS layer. For large angles between magnetizations, a rapid change of spin accumulation and spin current at the interface can be observed which leads to a large gradient of spin accumulation ($\Delta m$). The calculated spin accumulation and spin current are then used to determine the angular dependence of MR and subsequently the MR ratio can be obtained. As shown in figure 3, the results demonstrate that the MR significantly depends on the alignment of magnetization in both two ferromagnets. For the AP configuration where the relative angle is 180°, the MR value is notably higher whereas it becomes lower for the parallel state. The observed trend of the calculated MR is influenced by the arrangement of magnetization and closely aligns with the experimental study. This validation is essential for affirming the accuracy of the model and facilitating further studies.

We next investigate the effect of the current density injected into the structure, which is a critical factor influencing the behavior of spin transport and the resistance value of the magnetic structure due to spin scattering. A charge current is introduced perpendicular to the system, with a density ranging from 1.0 to 5.0 mA cm$^{-2}$. It is worth noting that the typical current density injected into CPP-GMR devices is on the order of 1 to 100 mA cm$^{-2}$. The exact value depends on the material, layer thickness, and device configuration. Higher current densities are often used to enhance spin-dependent scattering effects, leading to a better GMR ratio. However, very high current densities can also lead to heating, which is a critical factor affecting device performance and reliability. In practice, the Joule heating effect can be reduced by using heat sinks, good conductors, optimizing layer thickness and employing materials with high spin polarization, such as $Co_2FeSi$, which allows for lower current density and results in a low RA product.

The spatial variation of spin current and spin accumulation in both parallel and AP configurations is considered. The density of charge current significantly affects the spin current and spin accumulation within the magnetic structure. Injecting high current density into the system enhances the efficiency of spin transport between FMs, a key factor in generating spin accumulation. As demonstrated in figure 4, the RA product decreases with increasing current density. This indicates a higher efficiency of spin transport which subsequently leads to a higher MR ratio. Interestingly, utilizing Heusler alloys in magnetic structures, serving as pinned and FLs in read sensors, enables the device to operate at low current density while maintaining a high MR ratio. This observation aligns with both theoretical [38, 75] and experimental [38, 76–79] findings. Our study indicates that selecting suitable materials and optimizing current density can significantly enhance the performance

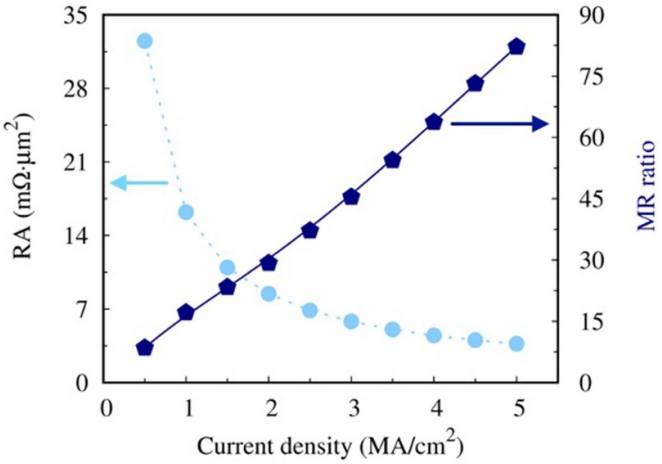


**Figure 4.** The resistance-area product and MR ratio in the trilayer system as a function of current density.

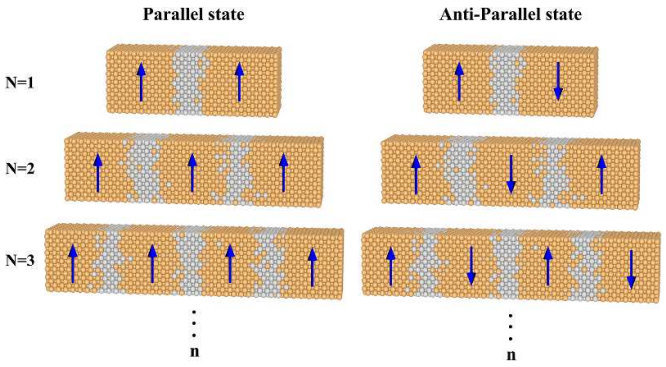


**Figure 5.** The parallel (P) and anti-parallel (AP) configurations of $(\mathrm{CFS/Ag/CFS})_{\mathrm{N}}$ structure.

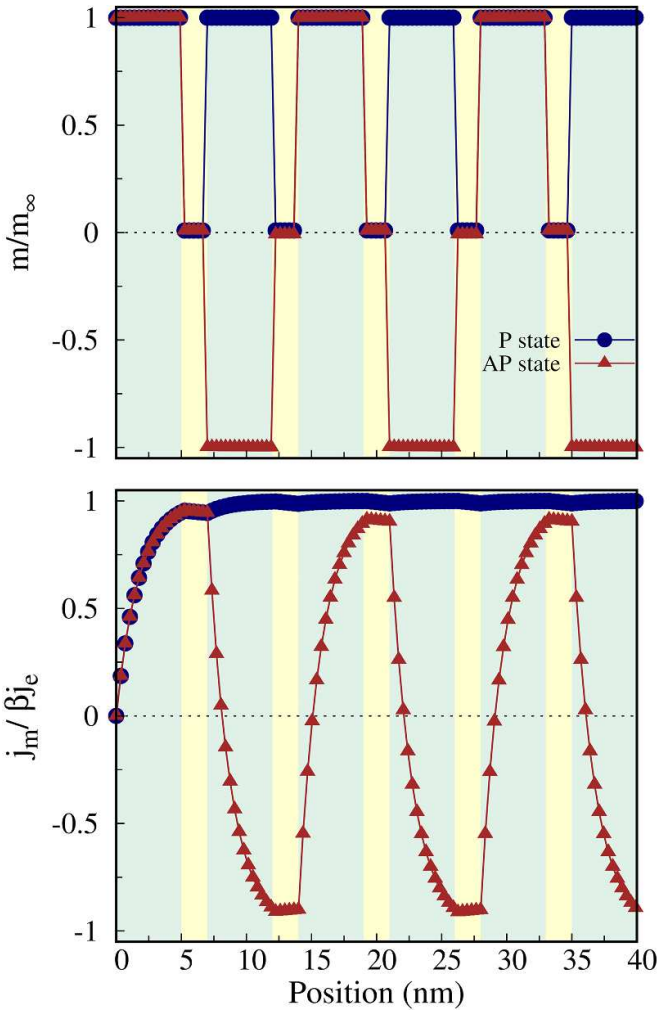


**Figure 6.** Spin accumulation in (a) P state and (b) AP state (C) spin current in the multilayer system of $(\mathrm{CFS/Ag/CFS})_5$.

of spintronic devices, which is essential for developing more efficient and reliable spintronic applications for practical use.

### *3.2. Spin transport in the multilayer structure*

In this part, we observe the spin transport behavior within the multilayer structure of $(\mathrm{CFS(5\,nm)/Ag(2\,nm)/CFS(5\,nm)})_{\mathrm{N}}$ to comprehend the underlying mechanisms of spin transport across various configurations. This finding can provide insights into optimal configurations for enhancing the performance of CPP-GMR sensors. The crystal structure of both CFS and Ag is characterized as face-centered cubic, with a lattice constant of 0.35 nm. The diffused interface between the materials is taken into account with approximately 1 nm thick. The system is divided into many thin layers allowing for a comprehensive analysis of the spatial variation of spin accumulation and spin current by applying the spin accumulation model. The MR ratio, indicating the performance of the read sensor in distinguishing between bit 0 and bit 1 can be obtained by considering the MR in both parallel (P) and AP configurations, as shown in figure 5.

A charge current with different densities is introduced into the multilayer system where the number of layers, $n$, varies from 1 up to 16. This study allows us to observe the effect of layer thickness and structure on the system's performance, enabling the scaling down of the system size while preserving high spin transport efficiency. The dynamics of magnetization in the system is considered by atomistic model and then the solution of spin accumulation and spin current in equations (2) and (3) are applied to the system. To simplify the explanation of the results, we provide an example for $N = 5$ with a current density of $j_e = 5\,\mathrm{mA\,cm^{-2}}$. As demonstrated in figure 6, it is found that the spin accumulation in the multilayer structure tends to align in the direction of magnetization, which is similar to the behavior observed in the trilayer structure CFS/Ag/CFS in the previous section. Interestingly, a rapid change in spin accumulation can be observed specifically at the interface between the CFS and Ag layers. This occurs due to differences in their spin transport properties. In addition, it can be explained that CFS exhibits high spin polarization and Ag provides efficient spin transport. The combined advantages of these two materials lead to enhanced changes in spin accumulation at the interfaces between CFS and Ag layers. In the multilayer system of CFS/Ag, the spin current

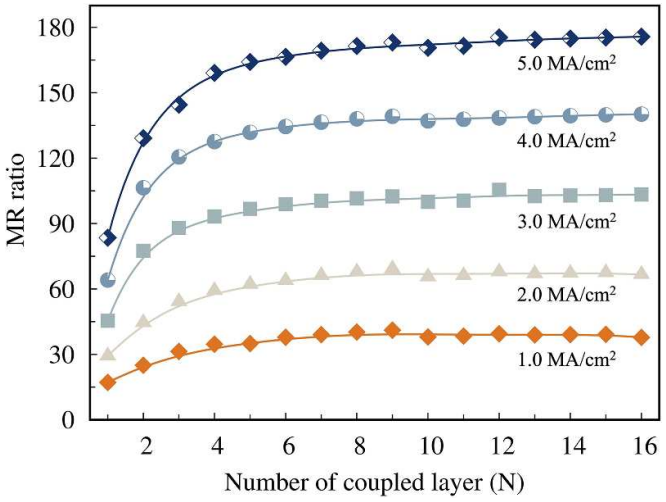


**Figure 7.** MR ratio in the multilayer system with different $N$ and current densities.

exhibits a development in the direction of magnetization in CFS layers due to their high spin polarization. Interestingly, in the parallel (P) state, it can be fully polarized at the value of the normalized spin current, $\beta j_e$ at a distance of approximately 10 nm, attributed to a short diffusion length scale of about 1.7 nm. In the Ag layers, the spin current flows continuously with only small changes, maintaining its magnitude throughout the Ag layer. This can be explained by the fact that the thickness of the CFS layer in the multilayer system influences the spin transport behavior [68]. Increasing the layer thickness increases the contribution of bulk spin scattering to the system and allows the spin current to become fully polarized. However, a thickness greater than the spin diffusion length may cause spin relaxation which reduces the spin transport efficiency. Therefore, a multilayer system is proposed to enhance device performance by increasing the contribution of interface scattering. Optimizing CFS thickness is crucial for maximizing spin transport efficiency.

Next, the gradient spin accumulation is derived from the simulated spin accumulation. Then, we determine the total RA for both the parallel (P) and AP states. This allows us to thoroughly evaluate the MR ratio, which is crucial for understanding the device's performance. As illustrated in figure 7, the number of coupled layers ($N$), corresponding to an increase in the number of interfaces within the multilayer structure, significantly influences the performance of CPP-GMR based sensors. This leads to elevated resistance within the system, particularly at the interfaces. This primarily arises from the enhanced scattering of spins at both the interfaces and within the bulk. The calculated findings reveal that increasing $N$ enhances both the resistance change and the MR ratio. Our results show a similar trend to previous studies [38, 80], showing the potential of Heusler alloy multilayers to enhance GMR for advanced read sensor applications. However, at the critical point $N = 5$, further increases do not significantly impact the MR ratio, which remains fairly constant. Interestingly, for $N$ greater than 5, the MR ratio doubles compared to when $N = 1$. These findings highlight the potential for improving the performance of multilayer CPP-GMR devices, offering advantages in designing and scaling down devices for enhanced functionality. Moreover, this study leads to substantial implications for the development of read sensors for the next generation of HDDs.

## 4. Conclusion

In summary, this study investigates Heusler alloy-based CPP-GMR sensors as a replacement for the TMR sensors currently used in HDDs, which are limited in achieving high areal density due to their large RA product. Understanding the physical mechanisms underlying the operation of CPP-GMR-based devices is important for enhancing their performance. This work focuses on CPP-GMR devices utilizing Heusler alloys by considering the $(\mathrm{CFS/Ag/CFS})_N$ multilayer system, including diffused interfaces. An atomistic model coupled with a spin accumulation model is employed. The atomistic model offers insights into the dynamic magnetization, while the spin accumulation model enables the calculation of the MR and MR ratios. This approach provides a comprehensive understanding of spin transport behavior within the structure. Our study starts by investigating the influence of injected current density, finding that increasing current density leads to a higher MR ratio. Subsequently, to optimize reader size and performance, we vary the number of coupled layers ($N$). The results demonstrate that increasing N enhances both the resistance change and MR ratio. However, at the critical point $N = 5$, further increases *in* $N$ do not impact the MR ratio and the MR ratio doubles compared to $N = 1$. These findings suggest the potential for enhancing the performance of multilayer CPP-GMR devices with optimal size.

## Data availability statement

The data that support the findings of this study are available upon reasonable request from the authors.

## Acknowledgments

P C and J C gratefully acknowledge the funding from Mahasarakham University and National Research Council of Thailand (NRCT) under the Grant No. NRCT5-RSA63014-01. R W C would like to acknowledge the support of the Mahasarakham University Development Fund.

## ORCID iDs

J Chureemart https://orcid.org/0000-0002-1318-9266
R W Chantrell https://orcid.org/0000-0001-5410-5615
P Chureemart https://orcid.org/0000-0002-1199-7809

## References

[1] Kubota Y *et al* 2018 *IEEE Trans. Magn.* **54** 1–6
[2] Wu H 2018 A study of the head disk interface in heat assisted magnetic recording - energy and mass transfer in nanoscale

[3] Koonkarnkhai S, Kovintavewat P and Keeratiwintakorn P 2015 *IEEE Trans. Magn.* **51** 1–4
[4] Murakoshi T, Komine T and Sugita R 2011 *Phys. Proc.* **16** 15
[5] Marchon B, Pitchford T, Hsia Y-T and Gangopadhyay S 2013 *Adv. Tribol.* (https://doi.org/10.1155/2013/521086)
[6] Albuquerque G, Hernandez S, Kief M T, Mauri D and Wang L 2022 *IEEE Trans. Magn.* **58** 1–10
[7] Lisiecki A and Król D 2020 Advertising strategy based on information growth in the zettabyte era *Advances in Computational Collective Intelligence. 12th Int. Conf. ICCCI 2020 (Proc.) (Da Nang, Vietnam, 30 November–3 December 2020)* ed M Hernes, K Wojtkiewicz and E Szczerbicki (Springer) pp 440–52
[8] Garani S S, Dolecek L, Barry J, Sala F and Vasić B 2018 *Proc. IEEE* **106** 286
[9] Mathew G, Hwang E, Park J, Garfunkel G and Hu D 2014 *IEEE Trans. Magn.* **50** 155
[10] Wood R, Miles J and Olson T 2002 *IEEE Trans. Magn.* **38** 1711
[11] Wang Y and Victora R H 2013 *IEEE Trans. Magn.* **49** 5208
[12] Barry J R, Vasic B, Khatami M, Bahrami M, Nakamura Y, Okamoto Y and Kanai Y 2016 *IEEE Trans. Magn.* **52** 1–7
[13] Kharwar S, Singh S and Jaiswal N K 2022 *IEEE Trans. Nanotechnol.* **21** 244
[14] Xin N *et al* 2023 *Nature* **616** 270
[15] Mopoung K and Sanorpim S 2019 *J. Magn.* **24** 437
[16] Coehoorn R 1995 Spin polarized electron transport *J. Magn. Magn. Mater.* **151** 341
[17] Inoue J 1996 *J. Magn. Magn. Mater.* **164** 273
[18] Hsu S Y, Barthélémy A, Holody P, Loloee R, Schroeder P A and Fert A 1997 *Phys. Rev. Lett.* **78** 2652
[19] Schuhl A and Lacour D 2005 *Comptes Rendus Physique* vol 6 (Spintronics) p 945
[20] Nagahama T, Yuasa S, Tamura E and Suzuki Y 2005 *Phys. Rev. Lett.* **95** 086602
[21] Dieny B 1992 *J. Phys.: Condens. Matter* **4** 8009
[22] Fujita Y, Miura Y, Sasaki T, Nakatani T, Hono K and Sakuraba Y 2021 *Phys. Rev.* B **104** L140403
[23] Chanda A *et al* 2023 *J. Magn. Magn. Mater.* **568** 170370
[24] Kübra Yildiz Aktaş B K A C B 2020 *J. Supercond. Novel Magn.* **33** 2093–100
[25] Li X, Su Y, Zhu M, Zheng F, Zhang P, Zhang J and Lü J-T 2021 *Phys. Rev. Appl.* **16** 034052
[26] Bakonyi I *et al* 2002 *J. Electrochem. Soc.* **149** 195
[27] Bakonyi I, Tóth J, Kiss L F, Tóth-Kádár E, Péter L and Dinia A 2004 *J. Magn. Magn. Mater.* **269** 156
[28] Péter L *et al* 2001 *J. Electrochem. Soc.* **148**
[29] Ennen I, Kappe D, Rempel T, Glenske C and Hütten A 2016 *Sensors* **16** 904
[30] Saeki R, Mizoguchi S, Kamimura H, Hayashida M and Ohgai T 2021 *J. Magn. Magn. Mater.* **529** 167849
[31] Coehoorn R 1991 *Phys. Rev.* B **44** 9331
[32] Samant M G *et al* 1994 *Phys. Rev. Lett.* **72** 1112
[33] Mosca D *et al* 1991 *J. Magn. Magn. Mater.* **94** L1
[34] de Gronckel H A M, Kopinga K, de Jonge W J M, Panissod P, Schillé J P and den Broeder F J A 1991 *Phys. Rev.* B **44** 9100
[35] Bird K D and Schlesinger M 1995 *J. Electrochem. Soc.* **142** L65
[36] Mardaneh M R, Almasi Kashi M and Ghaffari M 2022 *J. Alloys Compd.* **894** 162286
[37] Péter L, Pádár J, Tóth-Kádár E, Cziráki A, Sóki P, Pogány L and Bakonyi I 2007 *Electrochim. Acta* **52** 3813
[38] Shiroyama T, Sakuraba Y, Nakatani T, Sepehri-Amin H, Jung J W and Hono K 2018 *J. Appl. Phys.* **124** 163910
[39] gao Z, Chen J, Zhang Z, Liu Z, Zhang Y, Xu L, Wu J and Luo F 2023 *Adv. Electron. Mater.* **9** 2200823
[40] Angervo I, Saloaro M, Palonen H, Huhtinen H, Paturi P, Mäkelä T and Majumdar S 2022 *Appl. Surf. Sci.* **589** 152854
[41] Li F F *et al* 2005 *J. Appl. Phys.* **98** 113710
[42] Strelkov N, Vedyaev A, Ryzhanova N and Dieny B 2022 *J. Phys. D: Appl. Phys.* **56** 035001
[43] Kelvin Elphick M S T K K T H S S M, Frost W, Samiepour M, Kubota T, Takanashi K, Sukegawa H, Mitani S and Hirohata A 2021 *Sci. Technol. Adv. Mater.* **22** 235
[44] Anusree A C V, Rudenko N, Manivel Raja M and Kanchana V 2022 *Comput. Mater. Sci.* **213** 111625
[45] Yang T, Cao B X, Zhang T L, Zhao Y L, Liu W H, Kong H J, Luan J H, Kai J J, Kuo W and Liu C T 2022 *Mater. Today* **52** 161
[46] Sofi S A and Gupta D C 2020 *AIP Adv.* **10** 105330
[47] Johnson E D D, Suresh K G and Alam A 2016 *Phys. Rev.* B **94** 184102
[48] Hu J, Granville S and Yu H 2020 *Ann. Phys., Lpz.* **532** 1900456
[49] Aravindan V, Rajarajan A, Vijayanarayanan V and Mahendran M 2022 *Mater. Sci. Semicond. Process.* **150** 106909
[50] Ashwani Kumar D, Chandel T and Thakur N 2020 *Phil. Mag.* **100** 2721
[51] Bombor D *et al* 2013 *Phys. Rev. Lett.* **110** 066601
[52] Chatterjee S, Sau J, Samanta S, Ghosh B, Kumar N, Kumar M and Mandal K 2023 *Phys. Rev.* B **107** 125138
[53] Chatterjee S, Samanta S, Ghosh B and Mandal K 2023 *Phys. Rev.* B **108** 205108
[54] Manna K *et al* 2018 *Phys. Rev.* X **8** 041045
[55] Seh A Q and Gupta D C 2019 *Int. J. Energy Res.* **43** 8864
[56] Khamtawi R, Saenphum N, Chantrell R W, Chureemart J and Chureemart P 2023 *J. Phys. D: Appl. Phys.* **57** 135001
[57] Nakatani T M *et al* 2012 *IEEE Trans. Magn.* **48** 1751
[58] Chureemart P, Evans R F L, D'Amico I and Chantrell R W 2015 *Phys. Rev.* B **92** 054434
[59] Boonruesi W, Chureemart J and Chureemart P 2019 *Appl. Phys. Lett.* **115** 072408
[60] Boonruesi W, Chureemart J, Chantrell R W and Chureemart P 2020 *Phys. Rev.* B **102** 134427
[61] Chureemart J, pai S S a, Boonchui S, Chantrell R and Chureemart P 2021 *J. Magn. Magn. Mater.* **529** 167838
[62] Meo A, Sampan-a-pai S, Visscher P B, Chepulskyy R, Apalkov D, Chureemart J, Chureemart P, Chantrell R W and Evans R F L 2021 *Phys. Rev.* B **103** 054426
[63] Meo A, Chureemart J, Chantrell R W and Chureemart P 2022 *Sci. Rep.* **12** 3380
[64] Pai S S-A *et al* 2023 *Sci. Rep.* **13** 18474
[65] Phoomatna R, Sampan-a-pai S, Meo A, Chantrell R W, Chureemart J and Chureemart P 2024 *J. Phys. D: Appl. Phys.* **57** 185002
[66] Chureemart P, Cuadrado R, D'Amico I and Chantrell R 2013 *Phys. Rev.* B **87** 195310
[67] Chureemart P, D'Amico I and Chantrell R 2015 *J. Phys.: Condens. Matter* **27** 146004
[68] Saenphum N, Chureemart J, Chantrell R and Chureemart P 2019 *J. Magn. Magn. Mater.* **484** 238
[69] Saenphum N, Chureemart J, Evans R F L, Chantrell R W and Chureemart P 2021 *J. Phys. D: Appl. Phys.* **54** 395004
[70] Evans R F L *et al* 2014 *J. Phys.: Condens. Matter* **26** 144425
[71] Nakatani T M, Furubayashi T, Kasai S, Sukegawa H, Takahashi Y K, Mitani S and Hono K 2010 *Appl. Phys. Lett.* **96** 212501
[72] Furubayashi T, Nakatani T M, Goripati H S, Sukegawa H, Takahashi Y K, Inomata K and Hono K 2013 *J. Appl. Phys.* **114** 123910
[73] Huang H-L, Tung J-C and Guo G-Y 2015 *Phys. Rev.* B **91** 134409

[74] Saenphum N, Khamtawi R, Chureemart J, Chantrell R W and Chureemart P 2024 *Sci. Rep.* **14** 23925
[75] Prudnikov V V, Prudnikov P V and Romanovskiy D E 2016 *J. Phys. D: Appl. Phys.* **49** 235002
[76] Sanvito S, Lambert C J and Jefferson J H 2000 *Phys. Rev.* B **61** 14225
[77] Kwon B *et al* 2016 *J. Appl. Phys.* **119** 023902
[78] Geiersbach U, Bergmann A and Westerholt K 2003 *Thin Solid Films* **425** 225
[79] Furubayashi T, Kodama K, Nakatani T M, Sukegawa H, Takahashi Y K, Inomata K and Hono K 2010 *J. Appl. Phys.* **107** 113917
[80] Elsafi B 2024 *Indian J. Phys.* **98** 3469–74